Carbohydrate Polymers 373 (2026) 124622

Contents lists available at ScienceDirect

Carbohydrate Polymers

journal homepage: www.elsevier.com/locate/carbpol

Ionic agarose derivatives as polyelectrolytic additives for drug release

Markus Witzler [a,b,*], Margit Schulze [a,c], Martin Gericke [b,d,**], Thomas Heinze [b,e]

[a] Department of Natural Sciences, Bonn-Rhein-Sieg University of Applied Sciences, von-Liebig-Straße 20, 53359 Rheinbach, Germany
[b] Institute of Organic Chemistry and Macromolecular Chemistry, Friedrich Schiller University of Jena, Centre of Excellence for Polysaccharide Research, Humboldtstraße 10, 07743 Jena, Germany
[c] Faculty of Agriculture, Nutritional and Engineering Sciences, Rheinische-Friedrich-Wilhelms-University Bonn, Meckenheimer Allee 174, 53115 Bonn, Germany
[d] Robert Boyle Institute e.V., Im Steinfeld 10, 07751 Jena, Germany
[e] Posanova GmbH, Humboldtstraße 29, 99423 Weimar, Germany

ARTICLE INFO

Keywords:
Agarose derivatization
Agarose sulfates
Agarose phenylcarbonates
Agarose carbamates
Polyelectrolytes
Drug release
Release kinetics

ABSTRACT

Polysaccharides are being used as hydrogels for drug release in biomedical applications due to their inherent properties and biocompatibility. In this study, the synthesis, characterization, and application of ionic agarose derivatives are presented. Synthesis pathways for both anionic and cationic agarose derivatives with tunable degrees of substitution (DS) were established through homogeneous derivatization under mild conditions in ionic liquid. These derivatives partly retain their thermoreversible gelling behavior and can be used for polyelectrolyte systems. Agarose sulfates (AS) were synthesized in a one-step synthesis, while ammonium-bearing cationic agarose carbamates (AC) were synthesized via agarose phenylcarbonates (APC) with subsequent aminolysis. Both AS and AC were used in composite scaffolds of agarose and hydroxyapatite for sustained drug release into aqueous media. Layer-by-layer-coated alginate microbeads were prepared using oppositely charged agarose derivatives. Incorporating ionic agarose derivatives into these materials proved to effectively reduce the burst release and sustain the release of adenosine triphosphate (ATP), suramin, methylene blue, and A740003 over a time of 14 days. The release curves were evaluated using established models as well as two novel Langmuir-like models. Especially the latter two offered additional insight into the release and yielded higher scores in Akaike's Information Criterion rankings than commonly used models.

1. Introduction

Biomaterials play a major role in modern tissue engineering and drug delivery strategies. Derived from natural sources and mimicking original tissue composition they are often used as hydrogels, scaffolding material, and even as drug delivery system itself. The success of the used device heavily relies on the development of suitable biomaterial scaffolds that are not only cytotoxic but also provide additional features like controlling the release of therapeutic agents such as drugs, growth factors, or receptor ligands that enhance tissue growth (Kim & Tabata, 2015). Depending on the desired site of action, the materials used for scaffolds usually consist of biomimetic ceramics such as calcium phosphates and biopolymers (e.g. poly(lactic acid), alginate, or other polysaccharides) designed to work in synergy in order to meet both the desired structural requirements and the needed drug release features (Henkel et al., 2013; Hosseini et al., 2020; Koons et al., 2020). Usually, novel specifically tailored materials are required that combine high functionality with the requirements and high standards imposed for medical applications.

There are numerous strategies for controlling or sustaining the release of therapeutic agents in biomaterial-based systems (Abbadessa et al., 2024; Pei et al., 2024), depending on the drug, application site, target region, and the release system itself. Usually, the release is driven by diffusion or matrix degradation, where solubility of drug and matrix as well as matrix swellability are the main parameters that influence the release rate (Bruschi, 2015; Li & Mooney, 2016). A common way is drug encapsulation within hydrogel beads that can additionally be layered with oppositely charged polyelectrolytes ("layer-by-layer" / LbL approach) in order to prolong the release of the active ingredients due to electrostatic interaction (Kurapati et al., 2019; Neves et al., 2024; Wang et al., 2020). Among the biopolymers used for both scaffolds and release inhibitors, polysaccharides are specifically investigated, due to their inherent physico-chemical properties, general biocompatibility,

* Corresponding author at: Department of Natural Sciences, Bonn-Rhein-Sieg University of Applied Sciences, von-Liebig-Straße 20, 53359 Rheinbach, Germany.
** Corresponding author at: Institute of Organic Chemistry and Macromolecular Chemistry, Friedrich Schiller University of Jena, Centre of Excellence for Polysaccharide Research, Humboldtstraße 10, 07743 Jena, Germany.
E-mail addresses: markus.witzler@h-brs.de (M. Witzler), martin.gericke@uni-jena.de (M. Gericke).

https://doi.org/10.1016/j.carbpol.2025.124622
Received 3 February 2025; Received in revised form 8 October 2025; Accepted 29 October 2025
Available online 5 November 2025
0144-8617/© 2025 The Authors. Published by Elsevier Ltd. This is an open access article under the CC BY license (http://creativecommons.org/licenses/by/4.0/).

and possibility for chemical modification that offer specifically tailored materials (Kuznetsova et al., 2020; Malliappan et al., 2022).

Alginate, a polysaccharide found in brown algae, is already used for countless medical purposes, ranging from wound dressings over scaffold material in tissue engineering to drug delivery devices such as micro- and nanobeads (Uyen et al., 2020; Zhang et al., 2021). It is biodegradable, biocompatible, and forms ionotropic hydrogels with divalent cations. Agarose, another marine-derived polysaccharide, is a promising material for scaffolds and drug release systems due to its biocompatibility and reversible thermogelling behavior (Khodadadi Yazdi et al., 2020; Normand et al., 2000). Recent studies have explored its chemical modification, including the incorporation of functional groups and combination with other materials, to enhance drug release profiles and mechanical properties for biomedical applications (Khodadadi Yazdi et al., 2020). Additionally, it has been shown that agarose can be modified under homogeneous reaction conditions to introduce new functionalities (Gericke & Heinze, 2015; Gericke et al., 2024), where derivatives with low degrees of substitution (DS) may still exhibit thermoreversible gelation.

Numerous mathematical models for release evaluation have been established over time, some giving insight into the kinetic aspects or the transport mechanisms of the release, while others are purely mathematical descriptions of the release curves (Askarizadeh et al., 2023). Two of the most commonly used models for three dimensional release are the Korsmeyer-Peppas and Peppas-Salin models. They are valid up to 60 % of the respective release and offer detailed information on the speed of the release and the type of drug transport. Also common are the "First-Order" and Weibull models, which are not based on kinetic considerations, yet are still able to provide information that can be used to compare the amount of released drug and speed of the release. In a previous study, we have applied another mathematical model based on the Langmuir equation (Witzler et al., 2021), that can also be used for release evaluation.

This work is part of an ongoing project that aims to develop novel materials for the sustained release of drugs and purinergic receptor ligands that, in a future step, may be suited for guided stem cell differentiation. Hence, the target is to achieve a controlled release profile over a period of 14 days. Achieving these long release times for small hydrophilic drugs from hydrogel systems is currently a major challenge in drug release research (Neves et al., 2024). Four (model) drugs were selected for the study (see Fig. 1). Adenosine-5′-triphosphate (ATP), an active, non-selective P2 receptor ligand, is widely available and a structural key component of many other purinergic P2X and P2Y receptor ligands (Jacobson, 2010). Suramin is an active, non-selective P2 receptor ligand, which is both larger than ATP and carries different chemical moieties. In contrast to these two anionic drugs, methylene blue was employed as a cationic model drug for comparison. Finally, A740003 was included, which is an active, highly selective P2X7 antagonist (Honore et al., 2006; Wang et al., 2018). It is uncharged and less water-soluble compared to the other compounds. In our previous studies, hybrid scaffolds of hydroxyapatite and agarose were reported that showed a release of ATP and suramin in a timeframe of 3 to 4 days (Witzler et al., 2019). We have also reported on alginate beads that were coated with layers of commercially available polyelectrolytes and showed sustained drug release of ATP, suramin, and A740003 for up to 7 days (Witzler et al., 2021).

Based on the knowledge in the field of chemical modification of agarose and the fabrication of functional agarose and polysaccharide materials the following hypothesis were postulated and pursued in this study: (i) anionic and cationic agarose derivatives with low DS (≤ 0.5) as well as medium DS (≤ 1.0) can be prepared by suitable homogeneous synthesis methods, (ii) these polyelectrolytes can be incorporated into agarose-based scaffolds and LbL-coated alginate beads, and (iii) by tuning the molecular structure of the agarose derivatives it is possible to tune the interaction with drugs from the aforementioned materials and achieve a sustained release over up to 14 days. For curve-fitting and kinetic evaluation, we use well established mathematical models as well as two Langmuir-based models, which are then evaluated according to their ability to properly describe the data using Akaike's Information Criterion.

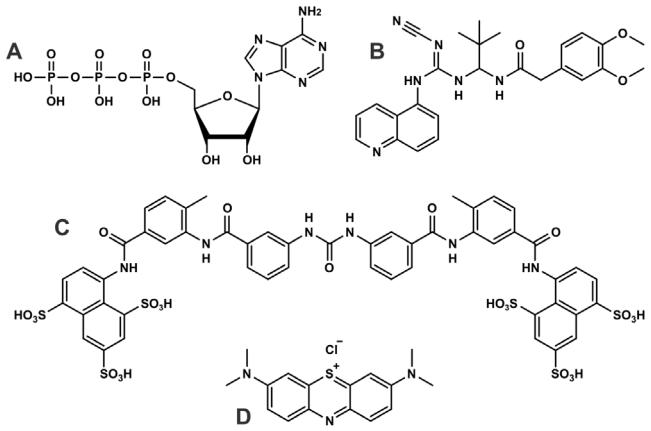

Fig. 1. Structural formulas of the model drugs under investigation. **A**: Adenosine-5′-triphosphate (ATP), **B**: A740003, **C**: suramin, **D**: methylene blue.

2. Experimental

2.1. Materials

Agarose (> 99 %, sulfate content 0.01 %, $M_w \approx 168\,500\,\mathrm{g\,mol^{-1}}$ (SEC method, Gericke & Heinze, 2015), $Đ = 2.19$, supplier code: 3810, LOT: 038266963), sodium alginate (for biochemistry, $M_w \approx 170\,000\,\mathrm{g\,mol^{-1}}$, $M/G = 1.14$), ATP (adenosine-5′-triphosphate disodium salt; 98 %), and Na_2CO_3 were purchased from Carl Roth GmbH & Co. KG (Karlsruhe, Germany). $Ca(NO_3)_2 \cdot 4\,H_2O$, $(NH_4)_2HPO_4$, NaOH, $CaCl_2 \cdot 2\,H_2O$, methylene blue, SO_3/pyridine complex, and CH_3I were purchased from Merck KGaA (Darmstadt, Germany). Suramin (hexasodium salt; > 98 %) and phenyl chloroformate (99 %) were bought from Alfa Aesar (Thermo Fisher GmbH, Kandel, Germany). A740003 ((*N*-[1-[[(cyanoamino)(5- quinolinylamino)methylene]amino]-2,2-dimethylpropyl]-3,4-dimethoxybenzene acetamide; > 96 %) was purchased from Alomone Labs (Jerusalem, Israel) and 1-butyl-3-methylimidazolium chloride (BMIMCl; 99 %) from iolitec GmbH (Heilbronn, Germany). Anhydrous *N*,*N*-Dimethylformamide (DMF) and pyridine were purchased from Acros Organics (Geel, Belgium) and stored as received. 3-(Dimethylamino)propylamine (> 98 %), ethanol, and tetrahydrofuran were bought from Sigma Aldrich (Taufkirchen, Germany). Deuterated solvents for NMR analysis (D_2O and DMSO-d_6) were purchased from Deutero GmbH (Kastellaun, Germany).

2.2. Measurements

FT-IR spectra were recorded on a Jasco FT/IR-410 spectrometer between 4000–500 $\mathrm{cm^{-1}}$ (32 scans, resolution: 1 $\mathrm{cm^{-1}}$) using KBr pellets containing 1 % of the solid polysaccharide. Spectra were smoothed using a Savitzky–Golay filter (2nd order polynome, 15 points) and normalized to [0, 1]. ^{1}H-NMR and ^{13}C{^{1}H}-NMR spectra were recorded in DMSO-d_6 with 16 scans or 10 000 scans respectively at 60 °C on a Bruker Avance I 250 MHz or Bruker Avance II 400 MHz spectrometer. A VARIO EL III CHNS analyzer was used for elemental analysis. The calculations for evaluating the degree of substitution (DS, for equations see Supporting Information) were based on the sulfur content for agarose sulfates and the nitrogen content for agarose carbamates. For agarose phenylcarbonates, which do not contain other heteroatoms, the DS were calculated from the region of aromatic protons in ^{1}H-NMR-spectra. Gelling behavior was tested in two ways: Each product was evaluated at a concentration of 10 $\mathrm{mg\,mL^{-1}}$ in water at both 25 °C

and 80 °C. For the samples that exhibited gel formation upon cooling, further rheologic measurements were conducted. Here, a HAAKE MARS III cone and plate viscosimeter (C35/2° Ti L, slit 105 µm) with a fixed shear rate of $\dot{\gamma} = 10\,s^{-1}$ and a temperature program was used. After applying the sample (20 mg mL^{-1}, dissolved at 95 °C and kept at 60 °C) to the pre-heated plate, the hood was closed and kept at 50 °C for 60 s. After this equilibration time, the temperature was cooled from 50 °C to 20 °C at a rate of 2 °C/min while measuring the viscosity. Measurements were stopped, when the rotating cone started to slip on the hardened gel. The gelation temperature was measured at the onset of the gelation, while the shear modulus was measured at the first plateau after gelation.

2.3. Synthesis

2.3.1. Synthesis of agarose sulfate (AS) in BMIMCl /DMF (*AS4*, typical example)

Dried agarose (3.00 g; 9.80 mmol repeating units, 1 eq.) was mixed with BMIMCl (27 g) and heated to 100 °C. After melting the ionic liquid and dissolving the agarose, the mixture was cooled to 80 °C. Next, 15 mL of dry DMF (5 mL DMF per g agarose) were added and the mixture was stirred for 1 h at 80 °C before it was cooled down to room temperature. SO_3/pyridine-complex (4.68 g; 29.4 mmol, 3 eq.) was dispersed in 15 mL of dry DMF, added to the reaction vessel, and stirred for 2 h. The product was precipitated in 300 mL ethanol, washed three times with 100 mL ethanol, and filtered. The isolated precipitate was then dissolved in ca. 50 mL of an aqueous solution of NaCl (2 %) at 80 °C. After neutralizing the solution with $NaHCO_3$, the product was precipitated in 200 mL ethanol/water (9:1), washed three times with 50 mL ethanol/water (9:1), filtered, and subsequently dried under vacuum at 60 °C.

Yield: 3.54 g white solid (8.99 mmol modified anhydro galactose unit (AGU), 91 % of theoretical yield) **AS4**.

DS_{SO_4} = 0.65 (from elemental analysis)

Elemental analysis: calculated (%) C: 38.7; H: 4.7; N: 0; S: 5.6; found (%) C: 37.8; H: 4.9; N: traces; S: 5.6.

$^{13}C\{^1H\}$-NMR (100 MHz, DMSO–d_6): δ (ppm) = 60.7 (G6), 65.3 (G6'), 68.1 (G4), 68.8 (LA6), 70.2 (G2,LA2), 73.2 (G5'), 75.0 (LA4), 75.4 (G5), 76.3 (LA5), 80.1 (LA3), 81.0 (G3), 97.5 (LA1), 102.2 (G1).

FT-IR (KBr): $\tilde{\nu}$ (cm^{-1}) = 3433 (s,br), 3218 (w), 2959 (w), 2898 (w), 1640 (m), 1476 (m,sh), 1401 (m), 1250 (s), 1160 (w), 1073 (s), 1006 (w), 930 (m), 890 (w), 817 (m), 773 (w).

2.3.2. Synthesis of agarose phenylcarbonate (APC) in BMIMCl /pyridine (*APC2*, typical example)

Dried agarose (2.00 g; 6.53 mmol repeating units, 1 eq.) was mixed with BMIMCl (18 g) and heated to 100 °C. After melting the ionic liquid and dissolving the agarose, the mixture was cooled to 80 °C. After addition of 5 mL dry pyridine (2.5 mL pyridine per g agarose), the mixture was stirred at 80 °C for at least 12 h. Then, additional 15 mL pyridine were added and the mixture was cooled to room temperature. Then, phenyl chloroformate (1.65 mL, 13.1 mmol, 2 eq.) was added dropwise and reacted for 3 h at room temperature. The product was obtained by precipitation into 500 mL of ice water, washed three times with 100 mL ice water and two times with 50 mL ethanol and separated via filtration. For purification, the solid was dissolved in 50 mL DMSO at 60 °C, precipitated into 200 mL ethanol, washed with ethanol, filtered, and dried under vacuum at 60 °C.

Yield: 2.08 g white solid (6.26 mmol modified AGU, 96 % of theoretical yield) **APC2**.

DS_{PC} = 0.24 (from NMR)

Elemental analysis: calculated (%) C: 49.0; H: 5.4; N: 0; S: 0; found (%) C: 48.1; H: 5.6; N: traces; S: 0.

$^{13}C\{^1H\}$-NMR (100 MHz, DMSO–d_6): δ (ppm) = 60.0 (G6), 67.4 (G4), 68.1 (LA6), 69.5 (G2,LA2), 74.3 (LA4), 75.5 (G5), 76.5 (LA5), 79.4 (LA3), 80.3 (G3), 96.8 (LA1), 101.5 (G1), 120.7 (C9 arom.), 125.8 (C11 arom.), 129.3 (C10 arom.), 150.6 (C8 arom.), 152.6 (C=O).

FT-IR (KBr): $\tilde{\nu}$ (cm^{-1}) = 3433 (s,br), 3218 (w), 2959 (w), 2898 (w), 1764 (m), 1640 (m), 1590 (w), 1490 (w), 1401 (m), 1258 (m), 1210 (s), 1160 (w), 1070 (s), 1022 (w), 930 (m), 890 (w), 773 (w).

2.3.3. Synthesis of agarose carbamate (AC) in DMF (*AC6* , typical example)

(3-Aminopropyl)trimethylammonium iodide (APTMAI) was prepared according to Gabriel et al. (2019). Briefly, 32 mL of 3-(dimethylamino)propylamine (DMAPA, 257 mmol, 1 eq.) were dissolved in 500 mL dry THF at 0 °C under nitrogen. Next, CH_3I (40.02 g, 282 mmol, 1.1 eq.) was added drop-wise and the mixture was stirred under nitrogen at 0 °C or 2.5 h. The product was filtered, washed five times with dry THF and dried under vacuum. The yellow product was stored under nitrogen atmosphere.

Agarose phenylcarbonate (APC5; 0.5 g; 1.3 mmol, 1 eq., DS_{PC} = 0.98) was dissolved in 25 mL dry DMF at 80 °C. After addition of APTMAI (1.55 g, 6.35 mmol, 5 eq.), the reaction mixture was stirred for 24 h at 80 °C. The product was isolated by precipitation into 150 mL ethanol, washed three times with 30 mL ethanol before filtration. The obtained solid was then dissolved in 40 mL H_2O and dialyzed for 72 h in H_2O (SpectraPor, MWCO 6000–9000 g mol^{-1}, threefold change of medium). After that, the solution was frozen at −40 °C and lyophilized to obtain a light-yellow solid.

Yield: 0.638 g light-yellow solid (91 % of theoretical yield) **AC6**.

DS_{CA} = 0.86 (from elemental analysis)

Elemental analysis: calculated (%) C: 41.0; H: 5.7; N: 4.4; I: 19.6; found (%) C: 38.7; H: 5.9; N: 4.4; I: 19.8.

$^{13}C\{^1H\}$-NMR (100 MHz, DMSO–d_6): δ (ppm) = 155.9 (C=O), 101.5 (G1), 96.9 (LA1), 80.3–67.4 (G2-4, LA2-6), 63.5 (–, CH_2, C10), 60.0 (G6), 52.4 (+, CH_3, C11), 37.5 (–, CH_2, C8), 22.9 (–, CH_2, C9).

FT-IR (KBr): $\tilde{\nu}$ (cm^{-1}) = 3431 (s,br), 2961 (w), 2895 (w), 1705 (m), 1640 (m), 1536 (m), 1479 (m), 1401 (m), 1258 (m), 1158 (w), 1070 (s), 967 (w), 930 (m), 894 (w), 771 (w).

2.4. Scaffold preparation and characterization

Pristine agarose gels (**A**) were prepared by dissolving agarose in water at 90 °C, pouring the solution into cylindrical molds and letting it cool down to room temperature. Agarose-based scaffolds mineralized with hydroxyapatite (**AH2**) were prepared according to a previously published method (Witzler et al., 2019). Briefly, an alkaline solution containing phosphate ions was slowly dropped into an agarose solution containing calcium ions at a temperature of 60–70 °C. The *in situ* generated hydroxyapatite was then cured at the same temperature for about 3 h, before the slurry was cast into cylindrical molds and allowed to cool down to room temperature. In case of samples **AH2S** and **AH2C**, half of the amount of agarose was substituted with ionic derivatives **AS3** or **AC3**, respectively. Cooled gels were then cut, frozen at −40 °C and lyophilized using a Alpha 2-4LD plus (Christ, Germany) at −82 °C and < 0.1 mbar.

2.5. Biocompatibility testing

Cooled gels with a diameter of 8 mm were cut to 1 mm height under sterile conditions, washed with deionized water, and conditioned in PBS buffer (pH 7.4) for 48 h before lyophylization. Nine of each lyophilized scaffold were then incubated for 76 h at 37 °C, 5 % CO_2 in a medium comprised of DMEM + 10 % fetal bovine serum + 100 U/mL/100 µg mL^{-1} penicillin/streptomycin. After incubation, the medium was collected and used for an MTT assay. Human mesenchymal stem cells (hMSCs) from adipose tissue of a 35-year old female donor (Lw35) were seeded into a 96-well plates at 20 000 and were incubated with scaffold-incubated medium for 16 h. Cells were then washed with PBS and cultivated with DMEM + additives (see above) + 0.5 mg mL^{-1} MTT for 4 h. DMSO was used for cell lysis and dissolution of formazan crystals. Cell viability was measured with a photometer (Anthos 2010, Biochrom Ltd., Cambridge, UK) at 550 nm.

2.6. "Layer-by-layer" -microbead preparation and characterization

Calcium alginate microbeads were prepared using a coaxial-spraying procedure and subsequently coated with five double-layers of agarose sulfate (**AS5**) and agarose carbamate (**AC6**) using a previously established procedure (Witzler et al., 2021). In short, for one double-layer, alginate beads were rinsed with ultrapure water, coated with 2 mL of the polycationic solution (2 % **AC6**) and vortexed for 1 min. After that, the beads were filtered, briefly rinsed with water, coated with 2 mL of the polyanionic solution (2 % **AS5**) and vortexed for 1 min, filtered, and then rinsed again with water.

For size determination of these "Layer-by-layer" (LbL) beads, static light scattering (SLS; Bluewave, Microtrac Europe, Germany, with Microtrac FLEX v.11.0.0.4 software) was used. For SLS experiments, approximately 200 mg of beads were used and sonicated for 1 min immediately before the measurement. For surface charge (ζ-potential) measurements, a Stabino Charge Titration System (colloid-metrix, Germany, with Stabino Control v.2.03.03 software) was used on 100–200 mg of the samples dispersed in 5 mL of water after each addition of either the polycation or -anion. The surface charge was determined by measuring the streaming potential in water at pH 5.5 caused by a moving piston periodically shearing the ionic double layer.

2.7. Drug loading

Four different model drugs were investigated in drug release experiments: two anionic substances adenosine-5′-triphosphate (ATP) and suramin, the cationic dye methylene blue, and the uncharged, functional P2X7 receptor ligand A740003. Lyophilized scaffolds were loaded via drop-in of a solution with known drug concentration and subsequent lyophilization. LbL-microbeads were loaded by adding the respective compound to the alginate solution prior to the bead formation. In order to prevent early release, the curing baths had the same concentration of drug as the alginate solution. Drug loading of the LbL-microbeads was determined by dissolving a known amount of beads in 0.5 M sodium carbonate solution and measuring the amount of incorporated drug via UV/Vis-spectroscopy at the drug's respective wavelength of the absorption maximum.

2.8. Drug release

Drug release into water at room temperature was monitored over a period of 14 days. Loaded scaffolds or microbead systems were placed into 20 mL of deionized water. The release containers were gently agitated throughout the release investigation. At given time intervals, 1 mL of medium was sampled and replenished with fresh water to keep a constant release volume. The concentration of the drug was measured photometrically at the drug's respective wavelength (λ_{ATP} = 255 nm, λ_{SUR} = 313 nm, λ_{MEB} = 660 nm, and λ_{A74} = 282 nm) and the overall released amount of drug was calculated.

From these data, a cumulative amount of drug released was calculated for each drug and each release system. All release experiments were performed in triplicates.

2.9. Release evaluation

For release data evaluation, all release curves were plotted cumulative release over time and subsequently fitted to different mathematical models using non-linear curve fitting in OriginPro 2016, OriginLabs, U.S.A. (built-in Levenberg–Marquardt algorithm, least-squares, max. 500 iterations, tolerance of 10^{-6}, no weighting). The mathematical models used were Korsmeyer-Peppas, Peppas-Sahlin, Weibull, First Order, a one stage and a two stage Langmuir-like model. The respective equations can be found in Table 1. A more detailed insight into the Langmuir-like models and the relationship between the mathematical model and their derivation is given in the Supporting Information. For curve fitting, the following constraints were given. Peppas-Salin model: $m = 0.45$ for cylindrical samples, $m = 0.43$ for spherical samples. Weibull model: $T = 0$ and $0 \leq M_\infty \leq 1$. "One-Stage" and "Two-Stage" models: none of the parameters N, B, S, T, T_B, or T_S can be zero. For each combination of drug and release material, a comparison of the model performances was done using the corrected Akaike's Information Criterion (AIC_c, eq. 1) for small sample sizes and relative Akaike weights (eq. 3) (Wagenmakers & Farrell, 2004).

$$AIC_c = N \cdot \ln \frac{RSS}{N} + 2P + \frac{2P^2 + 2P}{N - P - 1} \quad (1)$$

$$\Delta_i = AIC_c - AIC_{c_{min}} \quad (2)$$

$$w_i = \frac{\exp(-\Delta_i/2)}{\sum_{r=1}^{R} \exp(-\Delta_r/2)} \quad (3)$$

where N is the number of data points, P the number of parameters. Δ_i describes the distance between a model's AIC_c and the lowest AIC_c, while w_i describes the relative Akaike weight of a model, which can be interpreted as the model's probability to be the most parsimonious among the investigated models.

3. Results and discussion

3.1. Synthesis of ionic agaroses

A goal of this work was to synthesize both anionic and cationic agarose derivatives by defined chemical modification under homogeneous reaction conditions. Particular focus lay on the ability to tune the degree of substitution (DS) within the desired range (up to 1.0) and high yields for the products. Two synthesis routes were chosen (Fig. 2). Agarose sulfates (AS) were selected as anionic compounds and direct conversion of the polysaccharide in an ionic liquids was

Table 1
Overview on common release models as well as two novel Langmuir-like models. $\frac{M_t}{M_\infty}$ denotes the amount of drug released at time t, divided by the total amount of drug.

Model	Equation	Parameters
Korsmeyer-Peppas	$f(t) = \frac{M_t}{M_\infty} = K \cdot t^n$	K: release constant, n: type of diffusion
Peppas-Sahlin	$f(t) = \frac{M_t}{M_\infty} = K_1 \cdot t^m + K_2 \cdot t^{2m}$	K_1: release constant of diffusional release, K_2: release constant of relaxational release, m: fixed exponent from Korsmeyer-Peppas model depending on geometry
Weibull	$f(t) = \frac{M_t}{M_\infty} = 1 - exp\left[\frac{-(t-T)^b}{a}\right]$	T: release latency, a: curve scaling factor, b: curve shape factor, $\sqrt[b]{a} = t_{63.2}$: time to 63.2 % of the release
First Order	$f(t) = \frac{M_t}{M_\infty} = 1 - \exp(-k \cdot t)$	k: release rate
"One-Stage"	$f(t) = \frac{M_t}{M_\infty} = \frac{N_{max} \cdot t}{T + t}$	N_{max}: maximum released amount, T: half-time t_{50} until maximum released amount
"Two-Stage"	$f(t) = \frac{M_t}{M_\infty} = \frac{B \cdot t}{T_B + t} + \frac{S \cdot t}{T_S + t}$	B, S: maximum released amount for burst phase (B) and sustained phase (S), T_B, T_S: half-time t_{50} until respective maximum released amount for that phase

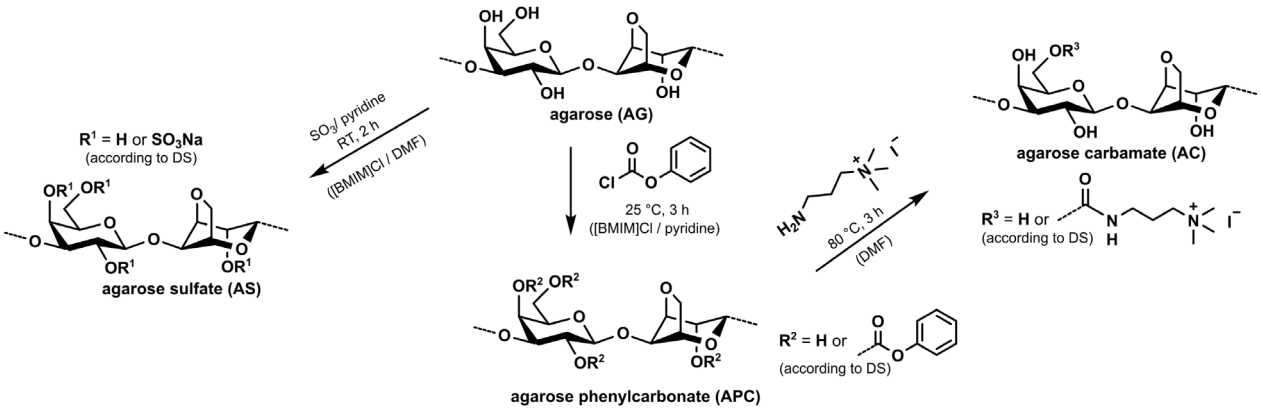

Fig. 2. Reaction scheme for the synthesis of agarose sulfate, agarose phenyl carbonate and the subsequent conversion in agarose carbamate.

studied. Agarose carbamates (AC) with a permanently charged quaternary ammonium group were selected as the cationic polyelectrolytes. The synthesis was achieved through aminolysis of previously prepared agarose phenylcarbonates (APC).

3.1.1. Synthesis and characterization of agarose sulfate

Agarose sulfates (AS) were synthesized using SO_3-pyridine complex (Fig. 2), which is a common reagent for sulfation of polysaccharides (Matsuhiro et al., 2014; Vogl et al., 2000). Usually, for agarose this reaction is carried out in dipolar aprotic solvents such as *N,N*-dimethylformamide (DMF) or *N,N*-dimethylacetamide (DMAc), requiring high temperatures ≥ 100 °C (Gericke et al., 2024) for agarose dissolution. Instead, an ionic liquid (1-butyl-3-methylimidazolium chloride / BMIMCl) was used as agarose solvent in this study, which allowed for milder dissolution conditions of 80 °C compared to previous reports. The sulfation of agarose in BMIMCl proceeded completely homogeneous and the resulting DS could be tuned in a range of about 0.2 to 1.0 by varying the molar ratio of the reagents (Table 2).

Agarose sulfates with a $DS < 0.6$ retained the thermo-gelling properties of pristine agarose, while agarose sulfates above $DS > 0.6$ were water-soluble even at room temperature. This is in accordance with previously published results by Vogl et al. (2000) on 1,4-*β*-D-galactan. Gelation temperatures of **AS1-3** measured at the onset of the gelation were about 2–3 °C lower than that of pristine agarose (36.8 °C) with shear moduli also being lower by a factor 2-7 (agarose: $G = 1.62$ mPa), respectively. These agarose sulfates are in the range of commercially available lower-gelling agarose (Kreimendahl et al., 2017; Normand et al., 2000).

No residuals of ionic liquid were detectable by elemental analysis or NMR spectroscopy. Peaks at wavenumbers 1250 cm^{-1} and 1073 cm^{-1} (characteristic for vibration) as well as peaks at 1006 cm^{-1} and 817 cm^{-1} (characteristic for S–O–C vibrations) were observed in the FT-IR spectra of AS samples (Fig. 3). This confirms that sulfate moieties were introduced into the agarose backbone. The ^{13}C-NMR spectra show a shift of the signal at 60 ppm that is corresponding to the G6 position to 65 ppm, which indicates a conversion at the primary hydroxy group at the agarose's G6 position (Gericke et al., 2024). For low DS with values below ≤ 0.65, the sulfation was found to be regioselective at G6, because no other additional peaks or shifts were observed. For high

Table 2
Conditions for and results of the synthesis of agarose sulfates (AS), agarose phenylcarbonates (APC), and agarose carbamates (AC).

Reaction conditions							Product						
starting material[a]	DS_{PC}[b]	solvent[c]	reagent[d]	molar ratio	T °C	t h	ID	DS[b]	yield %	reaction efficiency[e] %	solubility in H_2O[f] at 25 °C	rheology[g] T_{Gel} °C	G mPa
AG	–	IL/DMF	SO_3/Py	0.5	25	2	**AS1**	0.18	93	n.a.	–	34.0	0.88
AG	–	IL/DMF	SO_3/Py	1	25	2	**AS2**	0.49	80	n.a.	–	31.8	0.48
AG	–	IL/DMF	SO_3/Py	2	25	2	**AS3**	0.57	86	n.a.	–	33.0	0.24
AG	–	IL/DMF	SO_3/Py	3	25	2	**AS4**	0.65	91	n.a.	+		n.d.
AG	–	IL/DMF	SO_3/Py	5	25	2	**AS5**	0.91	95	n.a.	+		n.d.
AG	–	IL/Py	PhCF	1	25	3	**APC1**	0.12	96	n.a.	–	insoluble	
AG	–	IL/Py	PhCF	2	25	3	**APC2**	0.24	96	n.a.	–	insoluble	
AG	–	IL/Py	PhCF	3	25	3	**APC3**	0.52	93	n.a.	–	insoluble	
AG	–	IL/Py	PhCF	4	25	3	**APC4**	1.01	95	n.a.	–	insoluble	
AG	–	IL/Py	PhCF	5	25	3	**APC5**	0.98	93	n.a.	–	insoluble	
APC2	0.24	DMF	APTMAI	1	80	24	**AC1**	0.07	88	33	–	33.9	1.89
APC3	0.52	DMF	APTMAI	1	80	24	**AC2**	0.20	83	38	–	33.5	1.77
APC3	0.52	DMF	APTMAI	3	80	24	**AC3**	0.31	90	20	–	32.6	0.82
APC5	0.98	DMF	APTMAI	1	80	24	**AC4**	0.36	81	37	+		n.d.
APC5	0.98	DMF	APTMAI	3	80	24	**AC5**	0.69	88	24	+		n.d.
APC5	0.98	DMF	APTMAI	5	80	24	**AC6**	0.86	91	18	+		n.d.
APC4	1.01	DMF	APTMAI	1	80	24	**AC7**	0.40	81	38	+		n.d.

[a] AG: agarose; APC: agarose phenylcarbonate.
[b] DS: degree of substitution; PC: phenylcarbonate.
[c] IL: ionic liquid (1-butyl-3-imidazolium chloride); DMF: *N,N*-dimethyl formamide; Py: pyridine.
[d] SO_3/Py: sulfur trioxide/pyridine-complex; PhCF: phenyl chloroformate; APTMAI: (3-aminopropyl) trimethylammonium iodide.
[e] $DS_{CA}/(DS_{PC} \cdot molar\ ratio) \cdot 100\,\%$.
[f] evaluated at 10 mg mL^{-1}: + soluble; – insoluble.
[g] evaluated at 20 mg mL^{-1} in H_2O; T_{Gel} at onset of gelation; G at gel state; n.d.: not determined due to no gel formation.

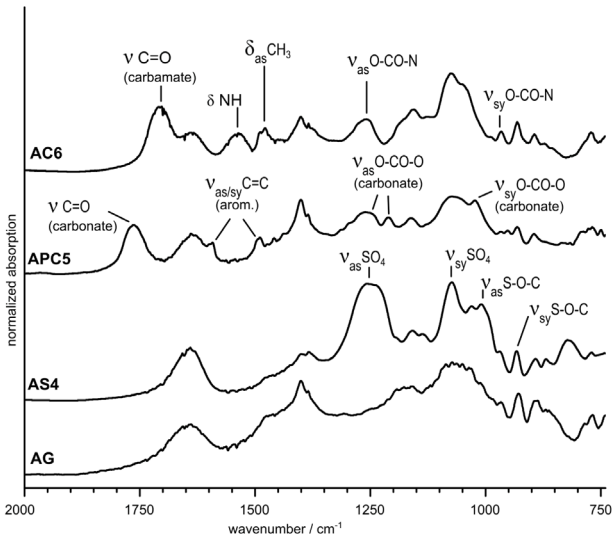

Fig. 3. Section of FT-IR spectra of agarose (**AG**), agarose sulfate (**AS**), agarose phenylcarbonate (**APC**), and agarose carbamate (**AC**) derived from **APC**.

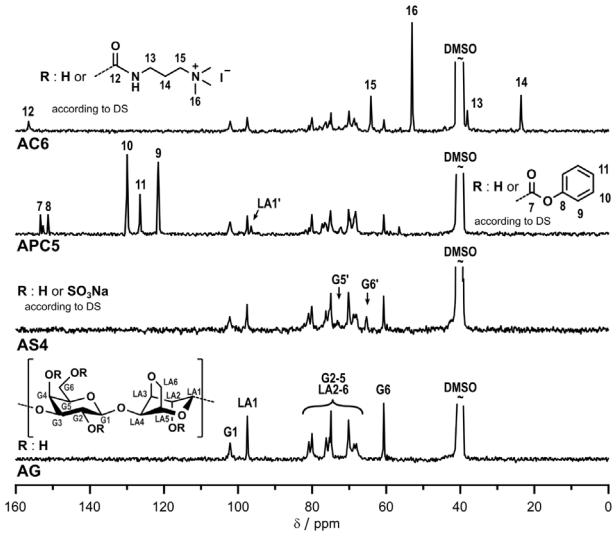

Fig. 4. ^{13}C-NMR spectra of agarose (**AG**), agarose sulfate (**AS**), agarose phenylcarbonate (**APC**), and agarose carbamate (**AC**) derived from **APC**, measured in DMSO-d_6 at 333 K.

DS of 0.91, a splitting of the peak around 98 ppm was observed that is corresponding to the carbon in position LA1. The splitting can be attributed to a partial sulfation at the neighboring LA2 position to a small extend.

Although the sulfation of polysaccharides using SO_3-pyridine complex has been widely used, there are only few dedicated studies on agarose or other galactans explicitly describing reaction conditions and resulting DS. Liang et al. (2014) reported a DS = 1.81 and sulfation of G6 and LA2 in a study focusing on carrageenans, but did not report the exact amount of chlorosulfonic acid used. Jie et al. (2012) reported sulfation of G6 and LA3 with DS = 0.17 and DS = 0.43 when using molar ratios of 4.5 and 9, respectively. Compared to our previous study using DMAc or DMAc/LiCl as main solvents (Gericke et al., 2024), using BMIMCl resulted in similar products with overall higher yields while applying milder dissolution conditions.

3.1.2. Synthesis and characterization of agarose carbamate

A modular two-step synthesis was chosen for the synthesis of cationic agarose derivatives (Fig. 2). It is based on the synthesis of reactive aryl polysaccharide carbonates followed by the conversion with a functional amine to yield a polysaccharide carbamate. The versatile approach has been studied extensively for polysaccharides such as dextran, cellulose, and xylan (Elschner et al., 2014; Gabriel et al., 2019). It has also been mentioned recently for the chemical derivatization of agarose (Gericke et al., 2024). However, DS values for the cationic products were rather low and no emphasis was placed on tailoring the DS values of the agarose derivatives. In the current work, the synthesis of tailored agarose phenylcarbonates (APC) and cationic agarose carbamates (AC) with well-defined DS values in the range of 0.1 and 1 could be obtained (Table 2). By adjusting the amount of phenyl chloroformate, it was possible to obtain APC with DS values between 0.12 and 1.01. However, increasing the amount of reagent to more then 4 equivalents did not result in a further increase in DS. This suggests that the conversion primarily occurs at the more reactive primary G6 position. All compounds were insoluble in water and soluble in organic solvents such as DMAc and DMF, which was expected considering that the aryl carbonate moiety is rather hydrophobic. The FT-IR spectra (see Fig. 3) revealed typical signals of characteristic vibrations in a carbonate group, especially the carbonyl stretching at 1764 cm^{-1}, the aromatic C=C vibrations at 1590 cm^{-1} and 1490 cm^{-1}, as well as the carbonate stretching at 1258 cm^{-1}, 1210 cm^{-1}, and 1022 cm^{-1}. ^{13}C-NMR spectra showed additional peaks in the downfield region that could be assigned to the phenyl carbonate moiety (Fig. 4). The peaks in the range of 120 to 130 ppm and 150 ppm were characteristic for aromatic carbon atoms in a phenolic ring. The peak at 152 ppm was assigned to the carbonyl group. Peaks in the range of about 60 to 80 ppm that were assigned to the agarose repeating unit only slightly changed. However, a small splitting of the peak at 100 ppm that was assigned to the LA1 carbon atom was observed for APC with a high DS of 1.0, which indicates conversion of the secondary LA2 position to a minor extent. This is in accordance with previous results (Gericke et al., 2024), where, although DS values vary slightly, the overall substitution pattern stays the same.

The APCs were then used for a subsequent aminolysis with (3-aminopropyl) trimethylammonium iodide (APTMAI), an ammonium-bearing amine in order to obtain a cationic AC derivative. Previous work have reported on the conversion of APC to AC using tetrahydrofuran as solvent (Seidi et al., 2015). However, DMF was use in this work due to the positive experiences with polysaccharide carbonates with different polymer backbone (including cellulose, dextran, xylan, and agarose) (Gabriel et al., 2019).

The conversion of APC with different starting DS of PC moieties was studied and 1 to 5 equivalents of amine were employed (Table 2). The resulting DS_{CA} were between 0.07 and 0.86 with yields above 80 % in all cases. The reaction efficiencies were between 18 and 38 % because a certain excess of amine was required to achieve complete conversion. The color of the products ranged from white for low DS to a yellowish color for higher DS. AC with a DS_{CA} > 0.35 were soluble in water, while those with lower DS retained the thermo-reversible gelling behavior. Gelation temperatures of **AC1-3** measured at the onset of the gelation were about 3–4 °C lower than that of pristine agarose (36.8 °C) with comparable or only slightly lower shear moduli (agarose: G = 1.62 mPa). The agarose carbamates have lower gelling temperatures but retain a higher modulus than the agarose sulfates **AS1-3**. Both FT-IR and ^{13}C-NMR spectra of the AC show only signals of the carbamate moieties, no signals of residual ionic liquid, and no or only minor peaks indicating residual carbonate moieties. This suggests a complete conversion of the carbonate moieties by aminolysis and partial hydrolysis. In the FT-IR spectrum (Fig. 3) the conversion is clearly visible at the shift of the carbonyl group related peak from 1764 cm^{-1} (carbonate) to 1705 cm^{-1} (carbamate), as well as the appearance of peaks at 1258 cm^{-1} and 967 cm^{-1} (O–CO–N structure vibrations) and 1479 cm^{-1} (methyl

group). The ^{13}C-NMR spectra (Fig. 4) also showed no remaining signals related to a phenylcarbonate group. Instead, a single peak for the carbonylic carbon atom appeared at 156 ppm. Moreover, peaks related to the methylene (22, 37, and 63 ppm) and the methyl groups (52 ppm) can now be identified. The single peaks for the carbonyl carbon atom and the carbon atom in LA1 position of agarose suggest that only the carbonate groups at the G6 position were converted into carbamates, while potential carbonates at the LA2 position hydrolyzed to hydroxy groups.

To summarize, previous reports have reported the synthesis AC derivatives with tertiary amino- and quaternary ammonium substituents (Gericke et al., 2024; Seidi et al., 2015) without residual ionic liquid. The present work provided further insight in the effect of different amounts of reagents and yielded products with a broader range of DS values from 0.1 to 0.9. Of particular note is that all compounds were soluble in water at elevated temperatures. Comparable polysaccharide carbamates with low DS < 1 were previously not accessible from polysaccharides with a primary hydroxy group in their repeating unit such as cellulose. The reason for this are side reactions that occur during the aminolysis of the corresponding aryl carbonates that result in crosslinking of the polymer chains (Gabriel et al., 2019). Apparently, these side reactions did not occur in the current case. A reasonable explanation might be the lower reactivity of APC in comparison to similar cellulose-based compounds as evidenced by the fact that the amount of amine require for complete aminolysis is higher as well (3 to 5 equivalents for APC vs. 1 to 3 equivalents for cellulose carbonates).

3.2. Scaffold and microbead preparation

The scaffolds and microbeads were prepared using previously published procedures (Witzler et al., 2019, 2021). Shortly, composite scaffolds were prepared using a gel casting method and lyophilization, while alginate microbeads were prepared by calcium gelation and a subsequent "Layer-by-Layer" (LbL) technique via immersion in polyelectrolyte solutions. Selected results of the characterization of the scaffolds and the microbeads are shown in Fig. 5, with panel A showing the results of the FT-IR measurements of the scaffold materials, panel B the biocompatibility results, and panels C-E showing the characterization of the microbeads, namely ζ-potential, size distribution, and digital micrographs.

The lyophilized scaffolds AH2, AH2C, and AH2S (agarose/hydroxyapatite composite, and composites with mixed-in carbamate and sulfate, respectively) were primarily characterized via FT-IR spectroscopy. The spectra (see Fig. 5A) show signals of both agarose (CH_2 and C–O–C vibrations) and hydroxyapatite (P–O vibrations) as well as the signals of the respective added ionic agarose. Here, for AH2C (agarose carbamate added), the signal at 1706 cm^{-1} corresponds to the carbonyl stretching of the carbamate group. For AG2S (agarose sulfate added), two signals at 1250 cm^{-1} and 1071 cm^{-1} can be allocated to characteristic sulfate vibration. These results suggest a proper integration of the ionic agarose derivatives into the composite scaffolds. The LbL-microbeads (LB) were evaluated on their surface charge (ζ-potential, see panel C) after each layer addition and size before and after layering. The addition of agarose carbamate resulted in $\zeta \approx 15$ mV, whereas the addition of a layer of agarose sulfate resulted in $\zeta \approx -18$ mV. This demonstrates the alternating layering of the polyelectrolytes onto the microbeads. Compared to the polyelectrolytes investigated previously (Witzler et al., 2021), agarose carbamate **AC6** yields comparable surface charges to chitosan but slightly less than poly(allyl amine). Agarose sulfate **AS5** yields slightly less surface charges than lignosulfonate but higher values than alginate. A size comparison unlayered alginate beads (**alg**) LbL-beads with five double layers (**LB**) of AC and AS is shown in panel D. There is no significant size difference between unlayered and layered beads, which can also been derived from the digital micrographs shown in panel E. The bead sizes are between 700–1100 µm, peaking around 900 µm and the layers only add thickness in the nanometer scale. Hence, these results are to be expected and are also in accordance with our previously published results on LbL-beads (Witzler et al., 2021), which did not exhibit significant changes in size, either. An MTT test on human mesenchymal stem cells (hMSC) of all scaffold materials, pristine, and layered beads was performed in order to evaluate biocompatibility (Fig. 5B). All materials performed comparable to the positive control, all clearly above the 70 % threshold according to ISO 10993-5:2009 for a successful biocompatibility testing (International Standards Organization, 2009). AH2C scaffolds exhibited the highest variation, which could indicate a sensitivity towards the carbamate moiety, however, the layered beads did not differ from the positive control group. In total, the results demonstrate that the materials are non-cytotoxic towards hMSC and are generally suitable for cell culture. It has to be noted though, that this study focuses on the materials and drug release and is limited to the general biocompatibility and does not provide results for a specific type of cell differentiation.

3.3. Drug release investigation

For drug loading of lyophilized scaffolds, the exact amount of drug added to the scaffold was noted and used as 100 % for the drug release calculations. The drug loading of the microbeads was determined after degradation of the beads. For the ionic drugs ATP, suramin, and methylene blue, the encapsulation efficiency was between 60–70 %, while that of A740003 was around 90 %. The exact values were used as 100 % for the drug release calculations and can be found in the Supporting Information (SI Table 1). The release of all four model drugs (see Fig. 1) has been monitored over a time span of 14 days. The cumulative drug release curves from all investigated systems are shown in Fig. 6. All release curves have been fitted with their best fitting mathematical model, which will be discussed in Section 3.3.2. Detailed values for the parameters of the fitted models can be found in the Supporting Information (SI section 2).

3.3.1. Evaluation of drug release curves

For the three ionic drugs (ATP, suramin, and methylene blue), the release from the scaffolds (Fig. 6 top row) is significantly slowed with the addition of hydroxyapatite to the agarose hydrogel. From a *burst release* of more than 90 % of drug released from unmodified agarose after 1 h, the release decreases to 50–90 % after addition of hydroxyapatite and the agarose derivative that is similarly charged like the drug, where the remainder of the drug is being released over the following two weeks. The release profiles still all feature a *burst release*, which makes the Peppas models well-applicable yielding plausible results for cylindrical release devices featuring a diffusion-driven release. The exponents of the Korsmeyer-Peppas fitting are generally below the optimum value of 0.45 for cylindrical release devices, indicating a diffusion-driven release with some additional effects such as different pore sizes, inhomogeneous drug distribution, or the fact that it is a three-dimensional release instead of a one-dimensional release, which the Korsmeyer-Peppas model assumes (Unagolla & Jayasuriya, 2018). However, with values being lower than the optimum, no indicators of a relaxational aspect of the release can be found (Malekjani & Jafari, 2021). For methylene blue, the model yield higher exponent values than 0.45, suggesting an abnormal diffusion. However, all Peppas-Sahlin ratios κ_1/κ_2 for diffusional and relaxational fractions of the release range from 4.6 to 20, confirming the high diffusional aspect of the release. Adding the ionic agarose oppositely charged to the drug to the agarose/hydroxyapatite system further decreases the *burst release* to around 20 % after 1 h. In this case, even after 14 days, only 40–70 % of the respective drug is released. Here, the "Two Stage"-model calculates only small *burst releases* of around 20 % (ATP, methylene blue) and 40 % (suramin) in the first day with t_{50} for the *sustained phase* of 25 to more than 50 days. The Peppas models still reveal a dominant diffusional release mechanism, only slower than for the other systems.

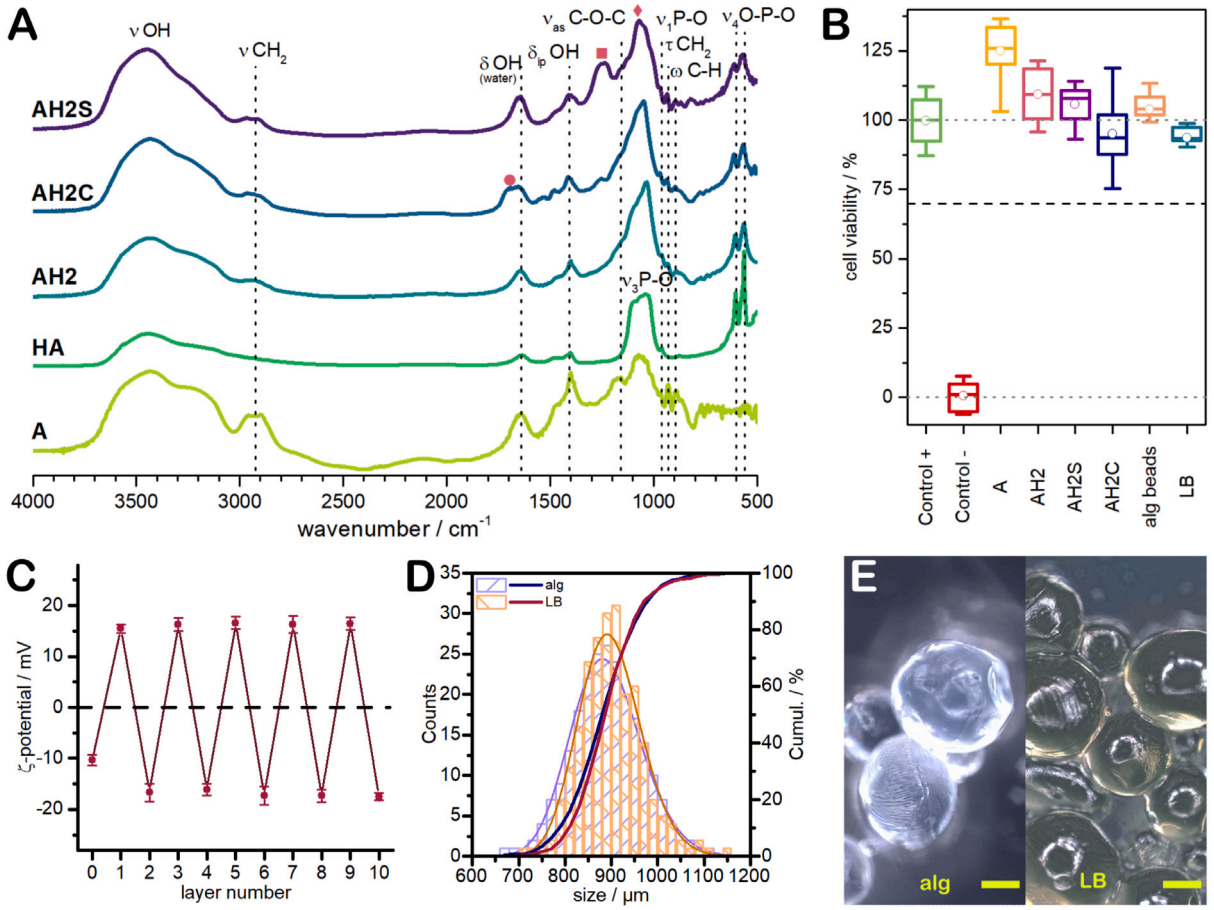

Fig. 5. Overview on the characterization of the different materials. **A**: FT-IR spectra of agarose, hydroxyapatite, and composite scaffolds without and with the ionic agaroses. Symbols in red mark specific signals of the ionic agaroses: • - carbamate carbonyl, ■- sulfate stretching, ♦ - sulfate stretching. **B**: cell viability data of all materials. MTT test on hMSC, $n = 9$. **C**: ζ-potential data of LB: layer 0 is the pristine alginate bead, odd layer numbers represent coatings with AC3, even layer numbers represent coatings with AS3. Mean ± SD, $n = 5$. **D**: size distribution and cumulative curves of pristine alginate beads and layered LB. **E**: digital micrographs of alginate beads and LB. Scale bars represent 250 µm.

The LbL-beads show a similar behavior: the beads itself already exhibit a slowed release with *burst release* between 40–60 %, which is in accordance with our previously published results on LbL-beads layered with commercially available polyelectrolytes (Witzler et al., 2021). Integration of the LbL-beads into (composite) hydrogels leads to a decreased *burst release* of 5–25 %. After that, the release behavior is almost linear up to 50 % after 14 days. Projected end times of the release (i.e. where the fit function reaches the value 1) are between 10 to 19 weeks. The general curve shapes as well as the parameters of the kinetic Peppas models (exponents $n \leq 0.40$ and high κ_1/κ_2 ratios) strongly suggest a diffusion-based release mechanism that is electrostatically hindered by the introduction of ionic groups from both the hydroxyapatite and the ionic agarose derivatives. Electrostatic interactions between drug and matrix have been described for various LbL-systems, which had a sustaining effect on the drug release (Hu et al., 2021; Verza et al., 2021). This is especially notable with suramin, which exhibits smaller κ_1/κ_2 ratios of around 1, indicating a much higher non-diffusional aspect of the release. Compared to conventional systems made from e.g. alginate and chitosan, the described agarose release systems perform remarkably better. For water-soluble drugs, the usual release periods are hours, rather than days. For example, Valdes et al. investigated the release of the phytohormone abscisic acid from alginate/chitosan systems. Depending on the exact composition, the release varied between 1 and 4 h (Valdes et al., 2024). In another study, water-soluble vitamin B12 was completely released from alginate/chitosan systems within 2 h at different pH values (Meskelis et al., 2024).

The less water-soluble drug A740003 shows a different release behavior. For the hydrogel scaffold systems, the release is independent of the system's composition: after 14 days, around 60 % of the drug is released. The release profiles feature a less pronounced *burst release* compared to the scaffold systems, however, the fitting models are able to identify a burst phase within the first day of release. For the LbL-beads, the release is almost completely inhibited, less than 10 % of the drug is released after 14 days, most of which is released in the first two days of the release investigation. This behavior suggests a release primarily driven by drug solubility instead of diffusion. In case of the LbL-beads, only small amounts near the surface are being released, while the rest of the drug remains inside of the capsule as long as it is not degraded. The Peppas models suggest a purely diffusion-driven release, however, they only take into account the first 60 % of each release curve, a region with very few data points and only very little released drug. Hence, it models only the small amount that is release via diffusion from near the surface of the beads. Other well-investigated release systems are comprised of alginate or chitosan or other natural polymers and polysaccharides. Curcumin is a common model drug used in release studies. Here, current studies are able to sustain the release to up to 2 days without burst release (Anirudhan et al., 2017), or producing tablets for intestinal delivery, which are able to sustain the release in gastric juices (Lin et al., 2024). In implant drug delivery, the alginate and chitosan systems are broadly used, often in conjunction with other materials to specifically tailor the properties and release behavior to the investigated problem (Farshidfar et al., 2023; Ribeiro et al., 2017). Release times of not or only slightly water-soluble

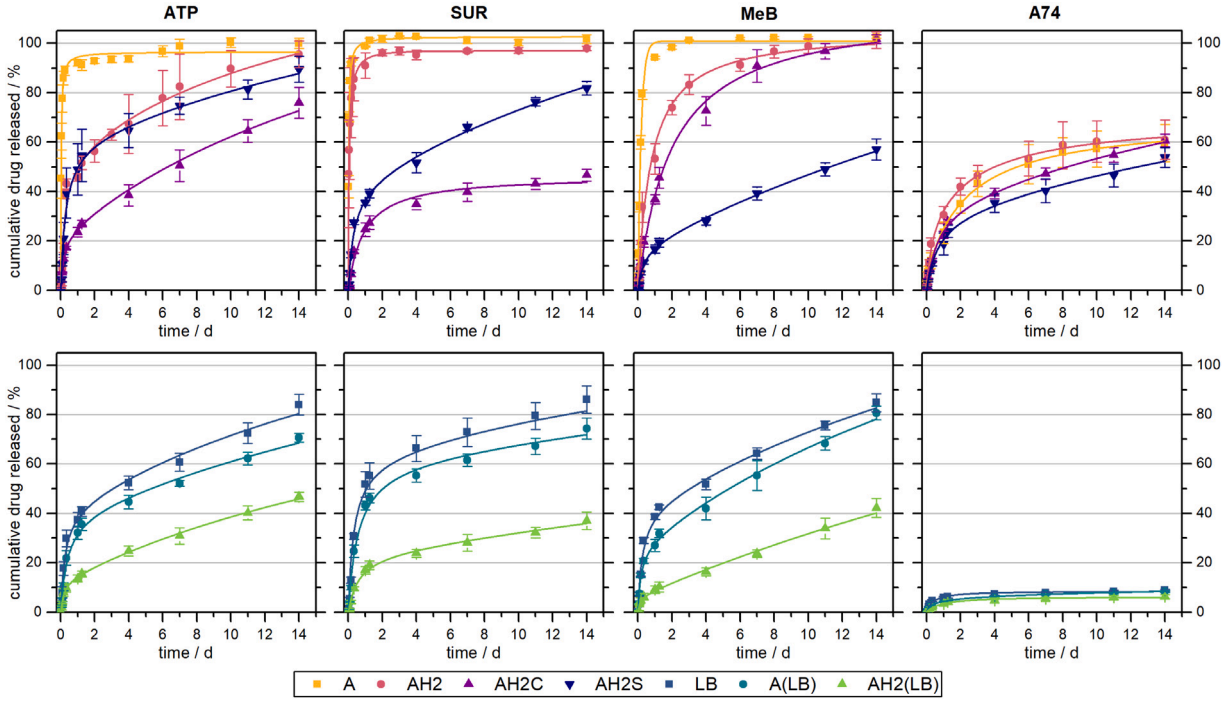

Fig. 6. Overview of drug release experiments. For each drug and system, the cumulative release is plotted over time. Mean value ± standard deviation. Fitted curve is the best fitting model according to the highest Akaike weight as shown in Fig. 7. **ATP**: adenosine triphosphate, **SUR**: suramin, **MeB**: methylene blue, **A74**: A740003. **A**: agarose, **AH2**: agarose/hydroxyapatite (33:67), **AH2C**: agarose/AC3/hydroxyapatite (16.5:16.5:67), **AH2S**: agarose/AS3/hydroxyapatite (16.5:16.5:67), **LB**: LbL-alginate beads, **A(LB)**: LbL-alginate beads embedded in agarose hydrogel, **AH2(LB)**: LbL-alginate beads embedded in AH2 hydrogel.

antibiotics range from several hours to up to 3 days (Hakim et al., 2021). Compared to these systems, the here described systems perform more inhibitory on the release of less water-soluble compounds, which was part of the study's objective.

For proper release evaluation the complete release curve has to be taken into account. Here, different established models as well as non-traditional models were used for non-linear curve fitting. All of the investigated models offer either direct kinetic insights (Peppas models, "First-Order") or at least descriptive parameters that give insight into the amount of drug released and a defined point in time, where a given amount of the drug is released (Weibull, "One Stage", "Two Stage"). The values for all of the models' parameters can be found in the Supporting Information (SI section 2). In cases with two distinct release phases, the "Two-Stage" model that is able to reflect two phases, generally yielded more detailed and more plausible results. In theory, the sum of the values B and S should be 1 for all models since not more than 100 % of drug can be released. However, in cases, where the second phase did not start to decrease yet, this expression is not fulfilled. Since constraining the fitting model to $B + S = 1$ did not result in successful fits, the times until $f(t) = 1$ (or respective maximum value)) were calculated (see SI Table 14). These values also represent the release sustaining effect of the incorporation of the ionic agarose derivatives. The release time was at least doubled (ATP in scaffolds) but could also reach values of up to three or more months (suramin in AH2(LB) and AH2C, as well as A740003). On the other hand, in the cases with visibly one phase, the traditional models often underestimated the maximum amount of released drug, which led to good performance of the "One-Stage" model. These results suggest that the incorporation of oppositely charged polyelectrolytes into the agarose gels is an effective way to prolong the release of ionic drugs, while maintaining the agarose's gelling behavior. Combining LbL-beads with agarose hydrogel systems prolongs drug release even further, although for non-ionic, less water-soluble drugs these systems might not be suitable as the release is not only prolonged but effectively inhibited.

3.3.2. Mathematical model evaluation

The mathematical models were ranked using the weights of the Akaike's Information Criterion (AIC_c) in order to select the most parsimonious model among those investigated (Wagenmakers & Farrell, 2004). Such a criterion is especially useful for multi-parametric non-linear curve-fitting, where a simple R^2 does not take the complexity of the model into account. The AIC_c evaluates the performance mainly on the *residual sum of squares* (RSS) and adds a penalty term for more complex models. The lowest AIC_c among the investigated models indicates the most parsimonious one. The Akaike weights are a useful tool to rank and compare the models of a given set by giving the relative distance to best performing model. The two Peppas models have been omitted for clarity, as they are only valid for the first 60 % of the respective release curves and are hence consequently ranked last by the AIC_c. The results of the AIC_c evaluation are displayed in Fig. 7, showing the ratios of the remaining four models under investigation. Tabulated values of the Akaike weights are shown in the Supporting Information (SI section 2).

In 26 out of 28 cases, one of the Langmuir-like models ("One Stage", teal, or "Two Stage", yellow) has been selected as the best fitting model, which underlines the great strength of these models to describe the release data. Only in two cases with high *burst release* a "First Order" or Weibull model is selected. In all cases where the release curve (Fig. 6) visually suggests only one release phase, the "One Stage"-model is the most parsimonious, while the profiles that suggest two distinct phases, namely a (small) *burst release* followed by a longer *sustained phase*, are being fitted best with the "Two Stage"-model. Although being descriptive models, the two Langmuir-like models can even offer some insight into the release kinetics. Their parameters account for the maximum amount of drug released and respective times until half of the drug is released for each stage. With that, they offer similar results to a Weibull model that also provides a maximum amount released and a time value (63.2 % released), which can be used to compare the speed of the drug release. However, in contrast to the Weibull model, the time value t_{50} in the Langmuir-based models, which is similar to a "half-life

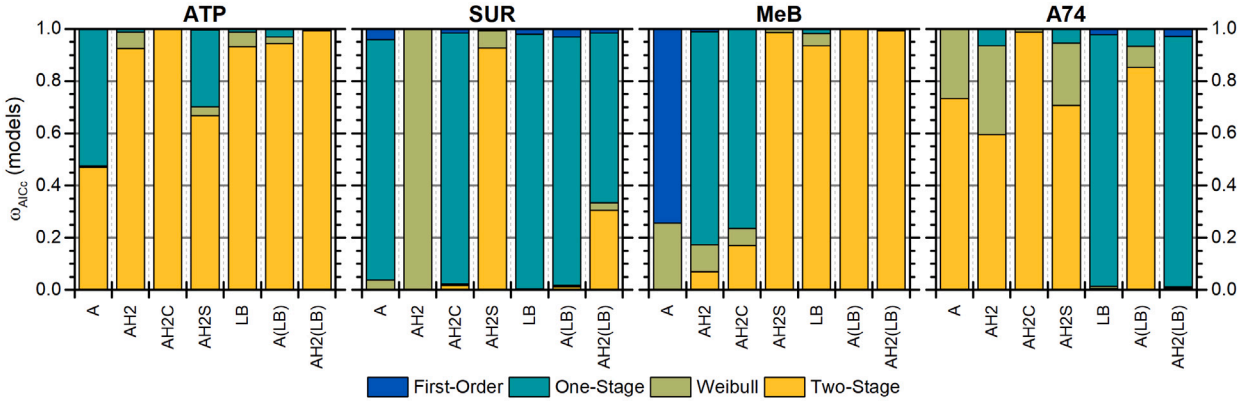

Fig. 7. Overview of Akaike weights for model selection. For each drug and system, the Akaike weight of every model is plotted. The larger the bar, the better fitting is the model. **A**: agarose, **AH2**: agarose/hydroxyapatite (33:67), **AH2C**: agarose/AC3/hydroxyapatite (16.5:16.5:67), **AH2S**: agarose/AS3/hydroxyapatite (16.5:16.5:67), **LB**: LbL-alginate beads, **A(LB)**: LbL-alginate beads in agarose hydrogel, **AH2(LB)**: LbL-alginate beads in AH2 mineralized hydrogel.

period", is easier to evaluate and far more approachable as it is part of the equation and not computed using two other fit parameters.

4. Conclusion

This study demonstrates the successful application of an ionic liquid as reaction medium for the homogeneous synthesis of ionic agarose derivatives with tuneable degrees of substitution (DS) between 0.1 and 1 and regioselective substitution on the primary hydroxy group for DS of up to 0.6. The resulting derivatives (agarose sulfates and ammonium-bearing agarose carbamates) include both water-soluble and gel-forming ionic agaroses, which were incorporated into drug delivery systems. By embedding gelling ionic agaroses into composite hydrogels, we achieved sustained release profiles for water-soluble model drugs, extending release times from several hours to over 14 days. Similarly, water-soluble ionic agaroses served as effective polyelectrolytes for alginate bead coatings, providing controlled release for ionic drugs while demonstrating inhibited release behavior for less water-soluble drugs. These findings are particularly significant for the sustained release of small hydrophilic drugs, where achieving long release times in aqueous systems remains a major challenge. The comprehensive kinetic evaluation, including the successful application of non-traditional Langmuir-like models and the use of an information criterion, further underscores the importance of robust mathematical modeling for accurately describing and optimizing drug release systems. Further research will focus on extending the derivatization strategy to achieve target DS values beyond 1, potentially unlocking new material properties and functionalities suitable for other applications than drug release. In addition, long-term release studies will be conducted to better characterize and model sustained release behavior over extended periods. Finally, *in vitro* release experiments with specific cell culture models will be essential in the future to further assess biocompatibility and optimal drug concentrations. Furthermore, the current limitation of cell differentiation experiments in the desired field of application should be addressed. Overall however, this work lays a solid foundation for the development of tailored drug delivery devices using ionic agarose derivatives, offering promising pathways for controlled and sustained drug release in pharmaceutical applications.

CRediT authorship contribution statement

Markus Witzler: Writing – original draft, Visualization, Methodology, Investigation, Formal analysis, Conceptualization. **Margit Schulze:** Writing – review & editing, Supervision, Resources, Funding acquisition, Conceptualization. **Martin Gericke:** Writing – review & editing, Validation, Methodology, Conceptualization. **Thomas Heinze:** Writing – review & editing, Software, Resources, Conceptualization.

Declaration of competing interest

The authors declare the following financial interests/personal relationships which may be considered as potential competing interests: Thomas Heinze reports a relationship with Posanova GmbH that includes: partial employment. Aside from that, the authors declare that they have no known competing financial interests or personal relationships that could have appeared to influence the work reported in this paper.

Acknowledgments

This work was funded by the German Federal Ministry of Education and Research (BMBF) program "Ingenieur Nachwuchs 2015": **PersoImplant** (grant no. 13FH019IX5), the Ministry of Culture and Science of the German State of North Rhine-Westphalia (MKW NRW) program "FH Zeit für Forschung 2016": **TestMedgO** (grant no. 1609FHZ027), and by the German Research Foundation (DFG) "Forschungsimpuls 26": **CytoTransport** (grant no. 528562393). This publication was partially funded by Bonn-Rhein-Sieg University of Applied Sciences. The authors thank C. Tonk, H-BRS for cell compatibility testing and M. Meurer, H-BRS for help with rheology testing.

Appendix A. Supplementary data

Supplementary material related to this article can be found online at https://doi.org/10.1016/j.carbpol.2025.124622.

Data availability

Data will be made available on request.

References

Abbadessa, A., Ronca, A., & Salerno, A. (2024). Integrating bioprinting, cell therapies and drug delivery towards in vivo regeneration of cartilage, bone and osteochondral tissue. *Drug Delivery and Translational Research*, *14*(4), 858–894. http://dx.doi.org/10.1007/s13346-023-01437-1.

Anirudhan, T. S., Anila, M. M., & Franklin, S. (2017). Synthesis characterization and biological evaluation of alginate nanoparticle for the targeted delivery of curcumin. *Materials Science and Engineering: C*, *78*, 1125–1134. http://dx.doi.org/10.1016/j.msec.2017.04.116.

Askarizadeh, M., Esfandiari, N., Honarvar, B., Sajadian, S. A., & Azdarpour, A. (2023). Kinetic modeling to explain the release of medicine from drug delivery systems. *ChemBioEng Reviews*, *10*(6), 1006–1049. http://dx.doi.org/10.1002/cben.202300027.

Bruschi, M. L. (2015). Strategies to modify the drug release from pharmaceutical systems, (1st ed.). (p. 208). Elsevier, http://dx.doi.org/10.1016/C2014-0-02342-8.

Elschner, T., Kötteritzsch, M., & Heinze, T. (2014). Synthesis of cellulose tricarbonates in 1-butyl-3-methylimidazolium chloride/pyridine. *Macromolecular Bioscience*, *14*(2), 161–165. http://dx.doi.org/10.1002/mabi.201300345.

Farshidfar, N., Iravani, S., & Varma, R. S. (2023). Alginate-based biomaterials in tissue engineering and regenerative medicine. *Marine Drugs*, *21*(3), 189. http://dx.doi.org/10.3390/md21030189.

Gabriel, L., Gericke, M., & Heinze, T. (2019). Modular synthesis of non-charged and ionic xylan carbamate derivatives from xylan carbonates. *Carbohydrate Polymers*, *207*, 782–790. http://dx.doi.org/10.1016/j.carbpol.2018.12.012.

Gericke, M., & Heinze, T. (2015). Homogeneous tosylation of agarose as an approach toward novel functional polysaccharide materials. *Carbohydrate Polymers*, *127*, 236–245. http://dx.doi.org/10.1016/j.carbpol.2015.03.025.

Gericke, M., Witzler, M., Enkelmann, A., Schneider, G., Schulze, M., & Heinze, T. (2024). Functional agarose hydrogels obtained by employing homogeneous synthesis strategies. *Polysaccharides*, *5*(June 2024), 184–197. http://dx.doi.org/10.3390/polysaccharides5030014.

Hakim, L. K., Yazdanian, M., Alam, M., Abbasi, K., Tebyaniyan, H., Tahmasebi, E., Khayatan, D., Seifalian, A., Ranjbar, R., & Yazdanian, A. (2021). Biocompatible and biomaterials application in drug delivery system in oral cavity. *Evidence-Based Complementary and Alternative Medicine*, *2021*(1), Article 9011226. http://dx.doi.org/10.1155/2021/9011226.

Henkel, J., Woodruff, M. A., Epari, D. R., Steck, R., Glatt, V., Dickinson, I. C., Choong, P. F. M., Schuetz, M. A., & Hutmacher, D. W. (2013). Bone regeneration based on tissue engineering conceptions — A 21st century perspective. *Bone Research*, *1*(3), 216–248. http://dx.doi.org/10.4248/BR201303002.

Honore, P., Donnelly-Roberts, D., Namovic, M. T., Hsieh, G., Zhu, C. Z., Mikusa, J. P., Hernandez, G., Zhong, C., Gauvin, D. M., Chandran, P., Harris, R., Medrano, A. P., Carroll, W., Marsh, K., Sullivan, J. P., Faltynek, C. R., & Jarvis, M. F. (2006). A-740003 [n-(1-[(Cyanoimino)(5-quinolinylamino) methyl]amino-2, 2-dimethylpropyl)-2-(3, 4-dimethoxyphenyl)acetamide], a novel and selective P2x7receptor antagonist, dose-dependently reduces neuropathic pain in the rat. *Journal of Pharmacology and Experimental Therapeutics*, *319*(3), 1376–1385. http://dx.doi.org/10.1124/jpet.106.111559.

Hosseini, E. S., Dervin, S., Ganguly, P., & Dahiya, R. (2020). Biodegradable materials for sustainable health monitoring devices. *ACS Applied Bio Materials*, *4*(1), 163–194. http://dx.doi.org/10.1021/acsabm.0c01139.

Hu, B., Guo, Y., Li, H., Liu, X., Fu, Y., & Ding, F. (2021). Recent advances in chitosan-based layer-by-layer biomaterials and their biomedical applications. *Carbohydrate Polymers*, *271*, Article 118427. http://dx.doi.org/10.1016/j.carbpol.2021.118427.

International Standards Organization (2009). *Biological evaluation of medical devices — Part 5: Tests for in vitro cytotoxicity*: *No. 10993-5:2009*, ISO, Geneva, Switzerland.

Jacobson, K. A. (2010). P2X and P2Y receptors. *Tocris Bioscience Scientific Review Series*, *33*, 1–15.

Jie, Y., Zhang, L., Chen, P., Mao, X., & Tang, S. (2012). Preparation of agarose sulfate and its antithrombogenicity. *Journal Wuhan University of Technology, Materials Science Edition*, *27*(1), 110–114. http://dx.doi.org/10.1007/s11595-012-0418-2.

Khodadadi Yazdi, M., Taghizadeh, A., Taghizadeh, M., Stadler, F. J., Farokhi, M., Mottaghitalab, F., Zarrintaj, P., Ramsey, J. D., Seidi, F., Saeb, M. R., & Mozafari, M. (2020). Agarose-based biomaterials for advanced drug delivery. *Journal of Controlled Release*, *326*, 523–543. http://dx.doi.org/10.1016/j.jconrel.2020.07.028.

Kim, Y.-H., & Tabata, Y. (2015). Dual-controlled release system of drugs for bone regeneration. *Advanced Drug Delivery Reviews*, *94*, 28–40. http://dx.doi.org/10.1016/j.addr.2015.06.003.

Koons, G. L., Diba, M., & Mikos, A. G. (2020). Materials design for bone-tissue engineering. *Nature Reviews Materials*, *5*(8), 584–603. http://dx.doi.org/10.1038/s41578-020-0204-2.

Kreimendahl, F., Köpf, M., Thiebes, A. L., Duarte Campos, D. F., Blaeser, A., Schmitz-Rode, T., Apel, C., Jockenhoevel, S., & Fischer, H. (2017). Three-dimensional printing and angiogenesis: Tailored agarose-type I collagen blends comprise three-dimensional printability and angiogenesis potential for tissue-engineered substitutes. *Tissue Engineering Part C: Methods*, *23*(10), 604–615. http://dx.doi.org/10.1089/ten.tec.2017.0234.

Kurapati, R., Groth, T. W., & Raichur, A. M. (2019). Recent developments in layer-by-layer technique for drug delivery applications. *ACS Applied Bio Materials*, *2*(12), 5512–5527. http://dx.doi.org/10.1021/acsabm.9b00703.

Kuznetsova, T. A., Andryukov, B. G., Besednova, N. N., Zaporozhets, T. S., & Kalinin, A. V. (2020). Marine algae polysaccharides as basis for wound dressings, drug delivery, and tissue engineering: A review. *Journal of Marine Science and Engineering*, *8*(7), http://dx.doi.org/10.3390/JMSE8070481.

Li, J., & Mooney, D. J. (2016). Designing hydrogels for controlled drug delivery. *Nature Reviews Materials*, *1*(12), 16071. http://dx.doi.org/10.1038/natrevmats.2016.71.

Liang, W., Mao, X., Peng, X., & Tang, S. (2014). Effects of sulfate group in red seaweed polysaccharides on anticoagulant activity and cytotoxicity. *Carbohydrate Polymers*, *101*(1), 776–785. http://dx.doi.org/10.1016/j.carbpol.2013.10.010.

Lin, J. T., Chiang, Y. C., Li, P. H., & Chiang, P. Y. (2024). Structural and release properties of combined curcumin controlled-release tablets formulated with chitosan/sodium alginate/HPMC. *Foods*, *13*(13), 2022. http://dx.doi.org/10.3390/foods13132022.

Malekjani, N., & Jafari, S. M. (2021). Modeling the release of food bioactive ingredients from carriers/nanocarriers by the empirical, semiempirical, and mechanistic models. *Comprehensive Reviews in Food Science and Food Safety*, *20*(1), 3–47. http://dx.doi.org/10.1111/1541-4337.12660.

Malliappan, S. P., Yetisgin, A. A., Sahin, S. B., Demir, E., & Cetinel, S. (2022). Bone tissue engineering: Anionic polysaccharides as promising scaffolds. *Carbohydrate Polymers*, *283*(January), Article 119142. http://dx.doi.org/10.1016/j.carbpol.2022.119142.

Matsuhiro, B., Barahona, T., Encinas, M. V., Mansilla, A., & Ortiz, J. A. (2014). Sulfation of agarose from subantarctic ahnfeltia plicata (ahnfeltiales, rhodophyta): Studies of its antioxidant and anticoagulant properties in vitro and its copolymerization with acrylamide. *Journal of Applied Phycology*, *26*(5), 2011–2019. http://dx.doi.org/10.1007/s10811-014-0297-3.

Meskelis, L., F. Agondi, R., Duarte, L. G., de Carvalho, M. D., Sato, A. C. K., & Picone, C. S. (2024). New approaches for modulation of alginate-chitosan delivery properties. *Food Research International*, *175*, Article 113737. http://dx.doi.org/10.1016/j.foodres.2023.113737.

Neves, B. S., Gonçalves, R. C., Mano, J. F., & Oliveira, M. B. (2024). Controlling the diffusion of small molecules from matrices processed by all-aqueous methodologies: Towards the development of green pharmaceutical products. *Green Chemistry*, *26*(8), 4417–4431. http://dx.doi.org/10.1039/D3GC04183B.

Normand, V., Lootens, D. L., Amici, E., & Plucknett, K. P. (2000). New insight into agarose gel mechanical properties. *Biomacromolecules*, *1*, 730–738. http://dx.doi.org/10.1021/bm005583j.

Pei, J., Yan, Y., Palanisamy, C. P., Jayaraman, S., Natarajan, P. M., Umapathy, V. R., Gopathy, S., Roy, J. R., Sadagopan, J. C., Thalamati, D., & Mironescu, M. (2024). Materials-based drug delivery approaches: Recent advances and future perspectives. *Green Processing and Synthesis*, *13*(1), Article 20230094. http://dx.doi.org/10.1515/gps-2023-0094.

Ribeiro, J. C. V., Vieira, R. S., Melo, I. M., Araújo, V. M. A., & Lima, V. (2017). Versatility of chitosan-based biomaterials and their use as scaffolds for tissue regeneration. *The Scientific World Journal*, *2017*(1), Article 8639898. http://dx.doi.org/10.1155/2017/8639898.

Seidi, F., Salarabadi, M. B., Saedi, S., Modadi, L., Shamsabadi, A. A., & Nikravesh, B. (2015). Introduction of a novel amino-agarose (AAG) derivative as a fixed facilitated transport carrier to prepare newly asymmetric PES/AAG membranes for CO 2 removal. *Greenhouse Gases: Science and Technology*, *5*(6), 701–713. http://dx.doi.org/10.1002/ghg.1514.

Unagolla, J. M., & Jayasuriya, A. C. (2018). Drug transport mechanisms and in vitro release kinetics of vancomycin encapsulated chitosan-alginate polyelectrolyte microparticles as a controlled drug delivery system. *European Journal of Pharmaceutical Sciences*, *114*(December 2017), 199–209. http://dx.doi.org/10.1016/j.ejps.2017.12.012.

Uyen, N. T. T., Hamid, Z. A. A., Tram, N. X. T., & Ahmad, N. (2020). Fabrication of alginate microspheres for drug delivery: A review. *International Journal of Biological Macromolecules*, *153*, 1035–1046. http://dx.doi.org/10.1016/j.ijbiomac.2019.10.233.

Valdes, O., Bustos, D., Guzmán, L., Muñoz-Vera, M., Urra, G., Castro, R. I., & Morales-Quintana, L. (2024). The controlled release of abscisic acid (ABA) utilizing alginate–chitosan gel blends: A synergistic approach for an enhanced small-molecule delivery controller. *Gels*, *10*(3), 185. http://dx.doi.org/10.3390/gels10030185.

Verza, B. S., van den Beucken, J. J., Brandt, J. V., Jafelicci Junior, M., Barão, V. A., Piazza, R. D., Tagit, O., Spolidorio, D. M., Vergani, C. E., & de Avila, E. D. (2021). A long-term controlled drug-delivery with anionic beta cyclodextrin complex in layer-by-layer coating for percutaneous implants devices. *Carbohydrate Polymers*, *257*, Article 117604. http://dx.doi.org/10.1016/j.carbpol.2020.117604.

Vogl, H., Paper, D., & Franz, G. (2000). Preparation of a sulfated linear (1→ 4)-β-d-galactan with variable degrees of sulfation. *Carbohydrate Polymers*, *41*(2), 185–190. http://dx.doi.org/10.1016/S0144-8617(99)00076-4.

Wagenmakers, E. J., & Farrell, S. (2004). AIC model selection using Akaike weights. *Psychonomic Bulletin and Review*, *11*(1), 192–196. http://dx.doi.org/10.3758/BF03206482.

Wang, N., Agrawal, A., Jørgensen, N. R., & Gartland, A. (2018). P2X7 receptor regulates osteoclast function and bone loss in a mouse model of osteoporosis. *Scientific Reports*, *8*(1), http://dx.doi.org/10.1038/s41598-018-21574-9.

Wang, S., Liu, R., Fu, Y., & Kao, W. J. (2020). Release mechanisms and applications of drug delivery systems for extended-release. *Expert Opinion on Drug Delivery*, *17*(9), 1289–1304. http://dx.doi.org/10.1080/17425247.2020.1788541.

Witzler, M., Ottensmeyer, P. F., Gericke, M., Heinze, T., Tobiasch, E., & Schulze, M. (2019). Non-cytotoxic agarose/hydroxyapatite composite scaffolds for drug release. *International Journal of Molecular Sciences*, *20*(14), 3565. http://dx.doi.org/10.3390/ijms20143565.

Witzler, M., Vermeeren, S., Kolevatov, R. O., Haddad, R., Gericke, M., Heinze, T., & Schulze, M. (2021). Evaluating release kinetics from alginate beads coated with polyelectrolyte layers for sustained drug delivery. *ACS Applied Bio Materials*, *4*(9), 6719–6731. http://dx.doi.org/10.1021/acsabm.1c00417.

Zhang, H., Cheng, J., & Ao, Q. (2021). Preparation of alginate-based biomaterials and their applications in biomedicine. *Marine Drugs*, *19*(5), 1–24. http://dx.doi.org/10.3390/md19050264.